Stress control of tensile-strained $In_{1-x}Ga_xP$ nanomechanical string resonators

Maximilian Bückle,[1] Valentin C. Hauber,[1] Garrett D. Cole,[2] Claus Gärtner,[2] Ute Zeimer,[3] Jörg Grenzer,[4] and Eva M. Weig[1,a)]
[1]*Department of Physics, University of Konstanz, D-78457 Konstanz, Germany*
[2]*Vienna Center for Quantum Science and Technology (VCQ), Faculty of Physics, University of Vienna, A-1090 Vienna, Austria*
[3]*Ferdinand-Braun-Institut, Leibniz-Institut für Höchstfrequenztechnik, D-12489 Berlin, Germany*
[4]*Institute of Ion Beam Physics and Materials Research, Helmholtz-Zentrum Dresden-Rossendorf, D-01328 Dresden, Germany*

(Received 29 August 2018; accepted 30 October 2018; published online 14 November 2018)

We investigate the mechanical properties of freely suspended nanostrings fabricated from tensile-stressed, crystalline $In_{1-x}Ga_xP$. The intrinsic strain arises during epitaxial growth as a consequence of the lattice mismatch between the thin film and the substrate, and is confirmed by x-ray diffraction measurements. The flexural eigenfrequencies of the nanomechanical string resonators reveal an orientation dependent stress with a maximum value of 650 MPa. The angular dependence is explained by a combination of anisotropic Young's modulus and a change of elastic properties caused by defects. As a function of the crystal orientation, a stress variation of up to 50% is observed. This enables fine tuning of the tensile stress for any given Ga content x, which implies interesting prospects for the study of high Q nanomechanical systems. *Published by AIP Publishing*. https://doi.org/10.1063/1.5054076

Introducing strain in material systems enables the control of various physical properties. Examples include the improved performance of semiconductor lasers,[1,2] enhanced carrier mobility in transistors,[3,4] direct formation of quantum dots,[5,6] and increased mechanical quality factors (Q) in micro- and nanomechanical systems (M-/NEMS).[7,8] In particular, tensile-strained amorphous silicon nitride has evolved to a standard material in nanomechanics in recent years. The dissipation dilution[9,10] arising from the inherent tensile prestress of the silicon nitride film gives rise to room temperature Q factors of several 100 000 at 10 MHz resonance frequencies,[7,8,11–13] while additional stress engineering has been shown to increase Q by a few orders of magnitude.[11,14,15] However, defects[16] set a bound on the attainable dissipation and hence Q in amorphous materials,[13,17,18] provided that other dissipation channels can be evaded.[13,19] Stress-free single crystal resonators, on the other hand, feature lower room temperature Q factors but exhibit a strong enhancement of Q when cooled down to millikelvin temperatures,[20] as a result of the high intrinsic Q of single crystal materials.[21] Combining dissipation dilution via tensile stress with high intrinsic Q of single crystal materials could open a way to reach ultimate mechanical Q at room temperature.

In recent years, a few possible candidates for tensile-strained crystalline nanomechanical resonators have emerged. Those include, for example, heterostructures of the silicon based 3C-SiC[22] and the III-V semiconductors GaAs,[23] GaNAs,[24] and $In_{1-x}Ga_xP$.[25] Advantages of ternary $In_{1-x}Ga_xP$ (InGaP) are the direct bandgap (for $x < 63\%$) and the broad strain tunability. When grown on GaAs wafers, this alloy system may be compressively strained, strain-free, or tensile strained, with possible tensile stress values exceeding 1 GPa, by varying the group-III composition x. The prospects of InGaP in nanomechanics range from possible applications in cavity optomechanics[25,26] to coupling with quantum-electronic systems, such as quantum wells[27] and quantum dots.[28]

Here, we explore freely suspended nanostrings fabricated from InGaP as nanomechanical systems. Our analysis reveals that even for fixed x, the tensile stress state of the resonator can be controlled by varying the resonator orientation on the chip. This implies that unlike for the case of silicon nitride NEMS, resonator orientation will be an important design parameter allowing us to fine-tune the tensile stress for any given Ga content x.

We investigate crystalline string resonators from two differently stressed, MBE grown III–V heterostructures, illustrated in Figs. 1(a) and 1(b). Both structures consist of two 86 nm thick InGaP layers, each capped by 1 nm of GaAs. Both InGaP layers are situated atop a sacrificial layer

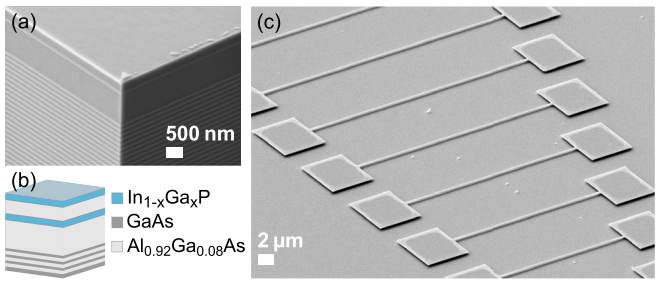

FIG. 1. Epitaxial heterostructure. Scanning electron micrograph (a) and schematic (b) of the employed heterostructure. Only the top InGaP and AlGaAs layers are used as the resonator and sacrificial layer, respectively. (c) String resonators with a thickness of 86 nm and lengths ranging from 9 μm to 53 μm. Micrographs in (a) and (c) show high-stress InGaP.

a)Electronic mail: eva.weig@uni-konstanz.de

of high aluminum content $Al_yGa_{1-y}As$ (AlGaAs), with $y = 92\%$. Note that only the top InGaP and AlGaAs layers were employed as the resonator and sacrificial layer, respectively, in this work.

By varying the Ga content of InGaP, the lattice-constant $a_L^\infty(x)$ changes by up to 7%. Since the substrate lattice constant of AlGaAs changes by only 0.1%, as a function of its Al content, we assume the lattice constant of AlGaAs to equal that of plain GaAs, $a_{AlGaAs} = a_{GaAs}$. The difference in lattice constants results in a lattice mismatch $\delta_L^\infty = (a_L^\infty(x) - a_{GaAs})/a_{GaAs}$ between the InGaP and the GaAs lattice. This mismatch induces an in-plane strain $\varepsilon^\parallel(x)$ in the InGaP layer and is defined by the ratio[29]

$$\varepsilon^\parallel(x) = \frac{a_L^\parallel - a_L^\infty(x)}{a_L^\infty(x)}, \quad a_L^\parallel = a_{GaAs} \tag{1}$$

with the distorted in-plane lattice constant $a_L^\parallel$ of the strained InGaP layer, which in the case of a 100% pseudomorphic layer equals the lattice constant of the substrate $a_L^\parallel = a_{GaAs}$. An InGaP layer grows strain-free (lattice-matched) on a GaAs substrate for the $x = 51\%$ Ga content, i.e., $a_L^\parallel = a_L^\infty(0.51)$.[25,30] The layer is grown tensile (compressive) strained for a higher (lower) Ga content. With this heterostructure, it is thus possible to adjust and tailor the strain in a film up to a critical thickness determined by x.[31,32] In this work, we investigate $In_{1-x}Ga_xP$ with Ga contents of $x_{HS} = 58.7\%$ (high-stress) and $x_{LS} = 52.8\%$ (low-stress). The resulting strain values are $\varepsilon^\parallel(x_{HS}) = 5.34 \times 10^{-3}$ and $\varepsilon^\parallel(x_{LS}) = 0.95 \times 10^{-3}$, for InGaP on GaAs, respectively.

String resonators were defined by electron-beam-lithography followed by a $SiCl_4$ inductively coupled plasma etch, using negative electron-beam-resist ma-N 2403 as an etch-mask, before releasing them with a buffered HF wet etch. The resonators are additionally cleaned via digital wet etching.[33] In the end, we critical-point dried the samples, to avoid stiction and destruction of the structures.[34] Examples of free standing string resonators are shown in Fig. 1(c).

The samples are explored at room temperature and mounted inside a vacuum chamber (pressure $< 10^{-3}$ mbar) to avoid degradation of the AlGaAs sacrificial-layer under ambient conditions[35] as well as gas damping. We measured the fundamental resonance frequency of the out-of-plane flexural mode of resonators of different lengths and orientations on the substrate, using piezo-actuation and interferometric detection. The InGaP resonators exhibit quality factors up to 70 000. Figure 2 presents the measured frequencies of several sets of resonators fabricated from the high-stress InGaP epitaxial structure as a function of the resonator length L for two different resonator orientations on the chip. Resonators with an angle of 0° are oriented parallel to the cleaved chip edges, see inset of Fig. 2, which correspond to the ⟨110⟩ crystal directions for III–V heterostructures on (001) GaAs substrate wafers. Hence, the strings point along a ⟨110⟩ direction. For comparison, we also discuss resonators which are rotated clockwise by 45° and hence are oriented along a ⟨100⟩ direction of the crystal.

Following Euler-Bernoulli beam theory,[36,37] we can express the eigenfrequency of the n-th harmonic as

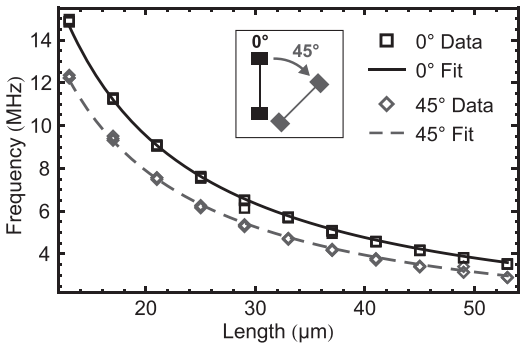

FIG. 2. Mechanical frequencies of stressed $In_{1-x}Ga_xP$, $x_{HS} = 58.7\%$, string resonators as a function of their length, for two different orientations on the chip. Resonance frequencies for 0°-resonators are plotted in black rectangles and resonators rotated clockwise by 45° in grey diamonds. Fits of both datasets show the $1/L$ frequency-dependence expected for the case of strongly prestressed string resonators. Calculating the weighted mean yields stress values of $\sigma(x_{HS}, 0°) = 642.3(3.3)$ MPa and $\sigma(x_{HS}, 45°) = 440.2(2.6)$ MPa. Inset: Resonator orientations with respect to chip edges.

$$f_n = \frac{n^2\pi}{2L^2}\sqrt{\frac{EI}{\rho A}}\sqrt{1 + \frac{\sigma A L^2}{n^2\pi^2 EI}}, \tag{2a}$$

$$f_n \approx \frac{n}{2L}\sqrt{\frac{\sigma}{\rho}} \quad \text{for} \quad \frac{\sigma A L^2}{n^2\pi^2 EI} \gg 1, \tag{2b}$$

where E is the Young's modulus, I is the area moment of inertia, ρ is the mass density, A is the cross-sectional area, and σ the stress. For the case of sufficiently strong tensile stress, Eq. (2a) reduces to Eq. (2b). The resonance frequencies shown in Fig. 2 are fitted with Eq. (2b) and clearly follow the expected $1/L$ dependence. Being in the high tensile stress regime, a change in frequency for a given resonator length can only originate from a different tensile stress σ. The frequency mismatch between the 0° and 45° data indicates that the stress depends on the resonator's orientation. Solving Eq. (2a) for σ and calculating the weighted mean from all data points yield $\sigma(x_{HS}, 0°) = 642.3(3.3)$ MPa and $\sigma(x_{HS}, 45°) = 440.2(2.6)$ MPa, indicating that the tensile stress varies by almost 50% with the crystal direction.

For anisotropic materials, stress σ and strain ε are related by the fourth rank compliance S or stiffness C tensors, $\sigma = C\varepsilon$ and $\varepsilon = S\sigma$.[38] For cubic crystals, those tensors simplify to 6×6 matrices with three independent components, c_{11}, c_{12}, and c_{44} (see supplementary material). For $In_{1-x}Ga_xP$, each component c_{ij} (x) depends on the Ga content x, and values are taken from Ref. 39.

By applying matrix rotations and transformations, one can calculate the angle dependent Young's modulus $E(x, \theta)$ of an ideal and defect free system (see supplementary material). Figure 3 shows $E(x, \theta)$ for the two different Ga contents $x_{HS} = 58.7\%$ and $x_{LS} = 52.8\%$. The Young's modulus displays a similar behavior for both Ga contents and varies between 80 GPa and 125 GPa, between the ⟨100⟩ and ⟨110⟩ crystal directions, respectively. In addition, Fig. 3 clearly reveals the 90° rotation symmetry of $E(x, \theta)$. To calculate the tensile stress, we multiply the Young's modulus by the strain from Eq. (1) according to Hooke's law

$$\sigma(x, \theta) = E(x, \theta)\varepsilon^\parallel(x). \tag{3}$$

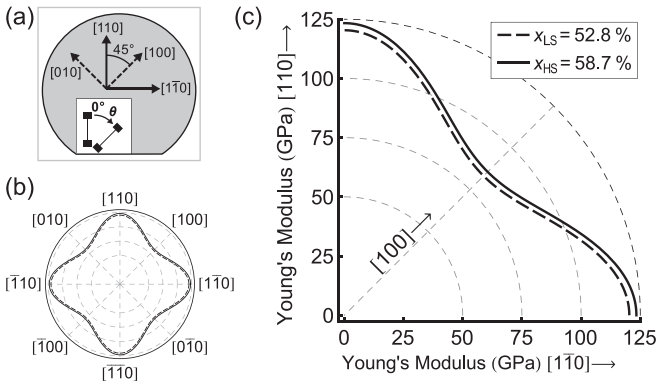

FIG. 3. Crystal orientation in wafers and angle dependent Young's modulus in $In_{1-x}Ga_xP$. (a) Schematic crystal orientations of a (001) GaAs wafer. In this case, unrotated (0°) resonators point along a ⟨110⟩ crystal direction. The resonator angles are changed clockwise, e.g., from [110] towards [100]. Inset: Definition of the resonator angle such that 0° resonators are parallel to the chip edge along a ⟨110⟩ direction. (b) Orientation dependent Young's modulus inside the (001) wafer plane, showing a 90° rotation symmetry. Solid line for $x_{HS} = 58.7\%$ and dashed line for $x_{LS} = 52.8\%$. (c) Close-up of angle dependent Young's modulus, showing the first quadrant of the polar plot (b).

The resulting stress values for both angles, $\sigma(x_{HS}, 0°) = 655.3\,\text{MPa}$ and $\sigma(x_{HS}, 45°) = 454.9\,\text{MPa}$, coincide well with the experimental results.

To further investigate the angular stress dependence of InGaP, we fabricated similar sets of resonators with angles changing in $\Delta\theta = 11.25°$ steps. For each orientation, the tensile stress is extracted using Eq. (2a). The top plots of Fig. 4 show the resulting angular stress dependence for two different Ga contents. In both cases, local stress maxima are observed at 0° and 90°, i.e., along ⟨110⟩ crystal directions. Accordingly, the minima are found at 45° and 135°, which correspond to ⟨100⟩ directions.

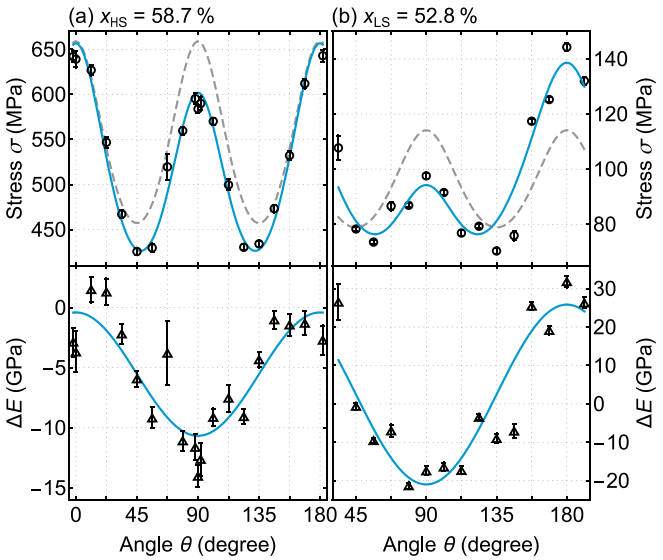

FIG. 4. Angular stress dependence of tensile strained $In_{1-x}Ga_xP$ string resonators. (a) High-stress InGaP with Ga content of $x_{HS} = 58.7\%$. Stress varying between 430 MPa and 640 MPa (top). Dashed gray line: Theoretically calculated stress, using Eqs. (1) and (3). Blue line: Taking a change of elastic properties due to defects into account by a $\cos(2\theta)$ angle dependent change ΔE of the Young's modulus $E(x, \theta)$ (bottom). (b) Low-stress InGaP with $x_{LS} = 52.8\%$. Showing a similar change of the Young's modulus as in (a). Error bars represent the uncertainty from the weighted mean calculation.

The gray dashed line in Fig. 4 depicts the stress values obtained by using Eqs. (1) and (3), which does not completely coincide with the experimental data. While the model conforms with the data at 0° and 180°, there are deviations around 90° for both $x_{HS} = 58.7\%$ and $x_{LS} = 52.8\%$.

To elucidate the deviation of stress, we have performed high resolution x-ray diffraction (HRXRD) reciprocal space map measurements[29] along two orthogonal ⟨110⟩ crystal directions as shown in Fig. 5(a). The diffraction peak arising from the InGaP layer lies directly above the substrate peak [circles in Fig. 5(a)], i.e., at the same $Q_{\langle 110\rangle}$ positions, and coincides with the expectation for a 100% pseudomorphic film within an accuracy of 10^{-3} Å^{-1}. In particular, the HRXRD measurements show the same out-of-plane strain for both the [110] and [$\bar{1}$10] sample orientations. However, the InGaP layer peaks show a different diffuse scattering which can be mainly attributed to point defects,[40] indicating different defect densities along the orthogonal ⟨110⟩ crystal directions.

Additional cathodoluminescence (CL) measurements in Fig. 5(b) are done to obtain further insight into the dislocation density in the epitaxial material. These measurements confirm different defect densities along the orthogonal ⟨110⟩ crystal directions. Dislocation lines have a higher density along the [$\bar{1}$10] direction than along [110].

It has been shown that defects can influence the elastic properties of crystalline materials and can lead to a softening as well as a hardening of the elastic constants.[41,42]

This change of elastic properties can be treated as an effective Young's modulus $\sigma(x, \theta)/\varepsilon^{\parallel}(x) = E(x, \theta) + \Delta E(\theta)$. We extract the deviation $\Delta E(\theta)$ from the experimentally obtained stress, the strain using Eq. (1), and the theoretically calculated Young's modulus determined in Fig. 3. The extracted values are shown in the bottom plots of Fig. 4 and clearly reveal an angular deviation from the theoretical Young's modulus. Both the softening and hardening of elastic constants can be seen for our two

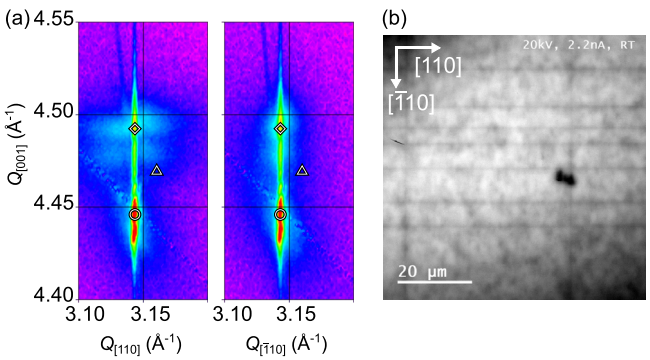

FIG. 5. (a) Reciprocal space maps depicting the asymmetric 224 reflections of the HRXRD measurement. On the left, the impinging x-ray beam is oriented along the [110] and on the right along the [$\bar{1}$10] direction. $Q_{[hkl]}$ are the reciprocal lattice vectors. The circle indicates the substrate peak. The layer peak position for a 100% pseudomorphic InGaP layer is indicated by a diamond. In contrast, the triangle indicates the position of a fully relaxed layer. The coincidence of the observed layer peak with the diamond confirms that the unstructured InGaP is 100% pseudomorphic. (b) Cathodoluminescence measurements are used to elucidate the dislocation density in the strained epitaxial structure. As shown in this image, the orthogonal ⟨110⟩ crystal directions exhibit a different density of dislocation lines (horizontal and vertical dark lines), resulting in variations of the defect structure as a function of orientation.

different InGaP compositions. One can see softening for the high-stress sample, while the low-stress sample shows both softening and hardening. Fitting a phenomenological $\cos(2\theta)$ function to the data leads to the deviation functions $\Delta E_{\mathrm{HS}}(\theta) = (-5.53 + 5.13\cos(2\theta))\,\mathrm{GPa}$ and $\Delta E_{\mathrm{LS}}(\theta) = (2.44 + 23.40\cos(2\theta))\,\mathrm{GPa}$, respectively. Adding those functions to the theoretical Young's modulus to calculate the angular stress [Eq. (3)], we obtain the solid blue lines in Fig. 4 which indicate the added effect.

In conclusion, we have explored tensile-strained nanomechanical string resonators fabricated from crystalline $In_{1-x}Ga_xP$. The initial InGaP thin film is pseudomorphically strained for a thickness of 86 nm and a Ga content of $x_{\mathrm{HS}} = 58.7\%$. For the given composition, we extracted an angle-dependent tensile stress of up to 650 MPa. InGaP with a Ga content of $x_{\mathrm{LS}} = 52.8\%$ shows lower tensile stress around 100 MPa with a similar angle-dependence as the high-stress InGaP. The observed angular stress dependence with respect to the crystal orientation is explained by a combination of anisotropic Young's modulus and a change of elastic properties caused by defects. This enables control over the stress of a nanomechanical resonator for a given heterostructure with fixed Ga content, which in turn could be optimized to enable maximum tensile stress. In addition, angular stress control opens a way to investigate the influence of tensile stress on the dissipation of nanomechanical systems. Stress control and further characterization of strained crystalline resonators will help to gain a deeper understanding in pursuit of ultimate mechanical quality factors.[14,15] Finally, InGaP is a promising material for cavity optomechanics, as two photon absorption is completely suppressed at telecom wavelengths.[25,26] Moreover, tensile strained InGaP could open a way to combine a high Q nanomechanical system with a quantum photonic integrated circuit on a single chip.[43,44]

See supplementary material for detailed descriptions of the fabrication process, calculations of the Young's modulus, comments on the critical thickness of the InGaP lattice matched to GaAs, and for more details on the HRXRD measurements.

G.D.C. would like to thank Chris Santana and the team at IQE NC for the growth of the epitaxial material used in this study. Financial support by the Deutsche Forschungsgemeinschaft via the collaborative research center SFB 767, the European Union's Horizon 2020 Research and Innovation Programme under Grant Agreement No 732894 (FET Proactive HOT), and the German Federal Ministry of Education and Research (contract no. 13N14777) within the European QuantERA co-fund project QuaSeRT is gratefully acknowledged.

The data and analysis code used to produce the nanomechanical plots are available at http://dx.doi.org/10.5281/zenodo.1477912.

[1]A. Ghiti, E. P. O'Reilly, and A. R. Adams, "Improved dynamics and linewidth enhancement factor in strained-layer lasers," Electron. Lett. **25**, 821–823 (1989).
[2]K. Y. Lau, S. Xin, W. I. Wang, N. Bar-Chaim, and M. Mittelstein, "Enhancement of modulation bandwidth in InGaAs strained-layer single quantum well lasers," Appl. Phys. Lett. **55**, 1173–1175 (1989).
[3]R. People, "Physics and applications of Ge(x)Si(1-x)/Si strained-layer heterostructures," IEEE J. Quantum Electron. **22**, 1696–1710 (1986).
[4]J. Welser, J. L. Hoyt, and J. F. Gibbons, "Electron mobility enhancement in strained-Si n-type metal-oxide-semiconductor field-effect transistors," IEEE Electron Device Lett. **15**, 100–102 (1994).
[5]D. Leonard, M. Krishnamurthy, C. M. Reaves, S. P. Denbaars, and P. M. Petroff, "Direct formation of quantum-sized dots from uniform coherent islands of InGaAs on GaAs surfaces," Appl. Phys. Lett. **63**, 3203–3205 (1993).
[6]L. Landin, M. S. Miller, M.-E. Pistol, C. E. Pryor, and L. Samuelson, "Optical studies of individual InAs quantum dots in GaAs: few-particle effects," Science **280**, 262 (1998).
[7]S. S. Verbridge, J. M. Parpia, R. B. Reichenbach, L. M. Bellan, and H. G. Craighead, "High quality factor resonance at room temperature with nanostrings under high tensile stress," J. Appl. Phys. **99**, 124304 (2006).
[8]T. Faust, P. Krenn, S. Manus, J. P. Kotthaus, and E. M. Weig, "Microwave cavity-enhanced transduction for plug and play nanomechanics at room temperature," Nat. Commun. **3**, 728 (2012).
[9]P.-L. Yu, T. P. Purdy, and C. A. Regal, "Control of material damping in high-Q membrane microresonators," Phys. Rev. Lett. **108**, 083603 (2012).
[10]G. I. González and P. R. Saulson, "Brownian motion of a mass suspended by an anelastic wire," Acoust. Soc. Am. J. **96**, 207–212 (1994).
[11]R. A. Norte, J. P. Moura, and S. Gröblacher, "Mechanical resonators for quantum optomechanics experiments at room temperature," Phys. Rev. Lett. **116**, 147202 (2016).
[12]A. H. Ghadimi, D. J. Wilson, and T. J. Kippenberg, "Radiation and internal loss engineering of high-stress silicon nitride nanobeams," Nano Lett. **17**, 3501–3505 (2017).
[13]L. G. Villanueva and S. Schmid, "Evidence of surface loss as ubiquitous limiting damping mechanism in SiN Micro- and nanomechanical resonators," Phys. Rev. Lett. **113**, 227201 (2014).
[14]Y. Tsaturyan, A. Barg, E. S. Polzik, and A. Schliesser, "Ultracoherent nanomechanical resonators via soft clamping and dissipation dilution," Nat. Nanotechnol. **12**, 776–783 (2017).
[15]A. H. Ghadimi, S. A. Fedorov, N. J. Engelsen, M. J. Bereyhi, R. Schilling, D. J. Wilson, and T. J. Kippenberg, "Elastic strain engineering for ultralow mechanical dissipation," Science **360**, 764–768 (2018).
[16]R. O. Pohl, X. Liu, and E. Thompson, "Low-temperature thermal conductivity and acoustic attenuation in amorphous solids," Rev. Mod. Phys. **74**, 991–1013 (2002).
[17]R. Rivière, S. Deléglise, S. Weis, E. Gavartin, O. Arcizet, A. Schliesser, and T. J. Kippenberg, "Optomechanical sideband cooling of a micromechanical oscillator close to the quantum ground state," Phys. Rev. A **83**, 063835 (2011).
[18]T. Faust, J. Rieger, M. J. Seitner, J. P. Kotthaus, and E. M. Weig, "Signatures of two-level defects in the temperature-dependent damping of nanomechanical silicon nitride resonators," Phys. Rev. B **89**, 100102 (2014).
[19]M. Imboden and P. Mohanty, "Dissipation in nanoelectromechanical systems," Phys. Rep. **534**, 89–146 (2014).
[20]Y. Tao, J. M. Boss, B. A. Moores, and C. L. Degen, "Single-crystal diamond nanomechanical resonators with quality factors exceeding one million," Nat. Commun. **5**, 3638 (2014).
[21]M. Hamoumi, P. E. Allain, W. Hease, E. Gil-Santos, L. Morgenroth, B. Gérard, A. Lemaître, G. Leo, and I. Favero, "Microscopic nanomechanical dissipation in gallium arsenide resonators," Phys. Rev. Lett. **120**, 223601 (2018).
[22]A. R. Kermany, G. Brawley, N. Mishra, E. Sheridan, W. P. Bowen, and F. Iacopi, "Microresonators with Q-factors over a million from highly stressed epitaxial silicon carbide on silicon," Appl. Phys. Lett. **104**, 081901 (2014).
[23]T. Watanabe, K. Onomitsu, and H. Yamaguchi, "Feedback cooling of a strained GaAs micromechanical beam resonator," Appl. Phys. Express **3**, 065201 (2010).
[24]K. Onomitsu, M. Mitsuhara, H. Yamamoto, and H. Yamaguchi, "Ultrahigh-Q micromechanical resonators by using epitaxially induced tensile strain in GaNAs," Appl. Phys. Express **6**, 111201 (2013).
[25]G. D. Cole, P.-L. Yu, C. Gärtner, K. Siquans, R. Moghadas Nia, J. Schmöle, J. Hoelscher-Obermaier, T. P. Purdy, W. Wieczorek, C. A. Regal, and M. Aspelmeyer, "Tensile-strained $In_xGa_{1-x}P$ membranes for cavity optomechanics," Appl. Phys. Lett. **104**, 201908 (2014).
[26]B. Guha, S. Mariani, A. Lemaître, S. Combrié, G. Leo, and I. Favero, "High frequency optomechanical disk resonators in III-V ternary semiconductors," Opt. Express **25**, 24639 (2017).
[27]E. A. Sete and H. Eleuch, "Controllable nonlinear effects in an optomechanical resonator containing a quantum well," Phys. Rev. A **85**, 043824 (2012).

[28]I. Wilson-Rae, P. Zoller, and A. Imamoğlu, "Laser cooling of a nanomechanical resonator mode to its quantum ground state," Phys. Rev. Lett. **92**, 075507 (2004).
[29]U. Pietsch, V. Holy, and T. Baumbach, *High-Resolution X-Ray Scattering: From Thin Films to Lateral Nanostructures (Advanced Texts in Physics)* (Springer, 2004).
[30]K. Ozasa, M. Yuri, S. Tanaka, and H. Matsunami, "Effect of misfit strain on physical properties of InGaP grown by metalorganic molecular-beam epitaxy," J. Appl. Phys. **68**, 107–111 (1990).
[31]J. W. Matthews, S. Mader, and T. B. Light, "Accommodation of misfit across the interface between crystals of semiconducting elements or compounds," J. Appl. Phys. **41**, 3800–3804 (1970).
[32]R. People and J. C. Bean, "Calculation of critical layer thickness versus lattice mismatch for Ge_xSi_{1-x}/Si strained-layer heterostructures," Appl. Phys. Lett. **47**, 322–324 (1985).
[33]G. C. DeSalvo, C. A. Bozada, J. L. Ebel, D. C. Look, J. P. Barrette, C. L. A. Cerny, R. W. Dettmer, J. K. Gillespie, C. K. Havasy, T. J. Jenkins, K. Nakano, C. I. Pettiford, T. K. Quach, J. S. Sewell, and G. D. Via, "Wet chemical digital etching of GaAs at room temperature," J. Electrochem. Soc. **143**, 3652–3656 (1996).
[34]J. Y. Kim and C.-J. Kim, "Comparative study of various release methods for polysilicon surface micromachining," in *Proceedings IEEE the Tenth Annual International Workshop on Micro Electro Mechanical Systems. An Investigation of Micro Structures, Sensors, Actuators, Machines and Robots* (1997), pp. 442–447.
[35]J. M. Dallesasse and N. Holonyak, "Oxidation of Al-bearing III-V materials: A review of key progress," J. Appl. Phys. **113**, 051101 (2013).
[36]W. Weaver, Jr., S. P. Timoshenko, and D. H. Young, *Vibration Problems in Engineering* (Wiley, 1990).
[37]A. N. Cleland, *Foundations of Nanomechanics: From Solid-State Theory to Device Applications* (Springer, 2002).
[38]M. A. Hopcroft, W. D. Nix, and T. W. Kenny, "What is the Young's modulus of silicon?," J. Microelectromech. Syst. **19**, 229–238 (2010).
[39]M. S. Shur, M. Levinshtein, and S. Rumyantsev, *Handbook Series on Semiconductor Parameters*, Ternary and Quaternary III–V Compounds Vol. 2 (World Scientific Publishing Co, 1999).
[40]V. M. Kaganer, R. Köhler, M. Schmidbauer, R. Opitz, and B. Jenichen, "X-ray diffraction peaks due to misfit dislocations in heteroepitaxial structures," Phys. Rev. B **55**, 1793–1810 (1997).
[41]S. Dai, J. Zhao, M-r He, X. Wang, J. Wan, Z. Shan, and J. Zhu, "Elastic properties of GaN nanowires: Revealing the influence of planar defects on Young's Modulus at nanoscale," Nano Lett. **15**, 8–15 (2015).
[42]Y. Chen, T. Burgess, X. An, Y.-W. Mai, H. H. Tan, J. Zou, S. P. Ringer, C. Jagadish, and X. Liao, "Effect of a high density of stacking faults on the Young's Modulus of GaAs nanowires," Nano Lett. **16**, 1911–1916 (2016).
[43]C. P. Dietrich, A. Fiore, M. G. Thompson, M. Kamp, and S. Höfling, "GaAs integrated quantum photonics: Towards compact and multi-functional quantum photonic integrated circuits," Laser Photonics Rev. **10**, 870–894 (2016).
[44]S. Bogdanov, M. Y. Shalaginov, A. Boltasseva, and V. M. Shalaev, "Material platforms for integrated quantum photonics," Opt. Mater. Express **7**, 111–132 (2017).